ACS OMEGA

http://pubs.acs.org/journal/acsodf

Article

Synthesis and Characterization of a Tertiary Composite of Cu, Mn, and g-C_3N_4: An Efficient Visible Light-Active Catalyst for Wastewater Treatment

Ali Raza Ayub, Asmat Ullah, Faisal Nawaz, Saqib Shafiq, Ahmed Abd El-Fattah, Hui Li,* and Javed Iqbal*

Cite This: *ACS Omega* 2023, 8, 19486−19493

Read Online

ACCESS | Metrics & More | Article Recommendations | Supporting Information

ABSTRACT: In this study, a tertiary composite of graphitic carbon nitride (GCN) with copper and manganese is utilized for photocatalytic degradation to add to efforts for tackling environmental pollution problems. The photocatalytic efficiency of GCN is enhanced with the doping of copper and manganese. This composite is prepared using melamine thermal self-condensation. The formation and characteristics of the composite Cu−Mn-doped GCN are affirmed by X-ray diffraction (XRD), scanning electron microscopy (SEM), ultraviolet (UV), and Fourier transform infrared spectroscopy (FTIR). This composite has been used for the degradation of an organic dye (methylene blue (MB)) from water at neutral conditions (pH = 7) of the solution. The percentage photocatalytic degradation of MB by Cu−Mn-doped GCN is higher than that of Cu−GCN and GCN. The prepared composite enhances the degradation of methylene blue (MB) from 5 to 98% under sunlight. The photocatalytic degradation is enhanced owing to the reduction of hole−electron recombination in GCN, enhanced surface area, and extended sunlight utilization by the doped Cu and Mn.

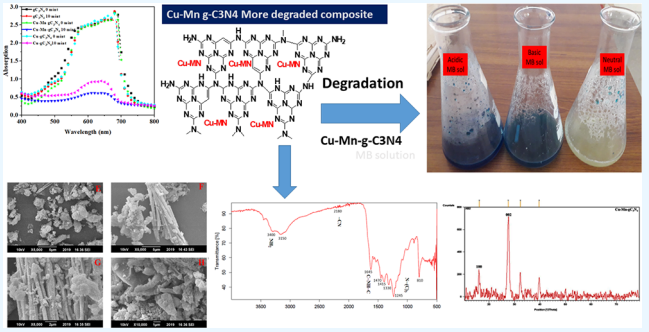

1. INTRODUCTION

The world is currently facing energy crisis and environmental contamination issues, which need to be addressed. The presence of many organic dyes as pollutants in water is dangerous not only for humans but also for the aquatic ecosystem.[1] In the past, various materials have been engaged in the photodegradation of organic pollutants that are present in the water.[1] Many methods are in place for wastewater treatment such as membrane separation, distillation, evaporation, adsorption, ozonation, ion exchange, aeration, chlorination, reverse osmosis, extraction, and advanced oxidation processes.[2] However, photocatalysis is among the new technologies used to decompose organic dyes from wastewater by hydroxyl radicals (OH^0) and is efficient among all the advanced oxidation (AO) processes.[2]

g-C_3N_4 (GCN) is one of the vital entities being easily available, highly stable, easy to fabricate, and low cost and bearing unique electronic structures, nontoxicity, and good intrinsic electron mobility and also shows a good response through the visible light field.[3,4] GCN has been used as a photocatalyst in microbial control, water disinfection, electrolyzing, and fuel cells.[3] The synthesis can be easily done by heating nitrogen-rich organic compounds, for example, urea [$CO(NH_2)_2$], thiourea (H_2NCSNH_2), melamine ($C_3H_6N_6$), cyanamide (CN_2H_2), and dicyanamide (C_2N^{-3}).[5] In the current study, we have used melamine as a precursor to synthesize GCN due to its low cost.[6,7] Although GCN is an efficient catalyst, its catalytic efficiency for the photodegradation of organic pollutants still needs to be improved.[6,8,9] Although many nonmetals such as B, C, N, O, S, P, F, and I have been doped on GCN to improve the photocatalytic activity, in comparison, doping of metals into GCN improves the catalytic efficiency 7−10 times.[4,9,10]

In the current work, we present a narrative synthetic way to prepare the Cu−Mn-doped GCN nanosheet by utilizing the Cu−Mn and melamine supramolecular network. Cu−Mn and melamine form a two-dimensional (2D) supramolecular network via hydrogen bonding. Photocatalytic activity of the Cu−Mn-doped GCN was demonstrated for photodegradation of the organic dyes methylene blue (MB) and RhB under visible irradiation, which showed improved catalytic performance. X-ray diffraction (XRD), Fourier transform infrared

Received: February 8, 2023
Accepted: May 10, 2023
Published: May 23, 2023

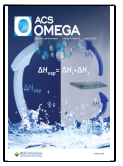

ACS Publications

© 2023 The Authors. Published by American Chemical Society

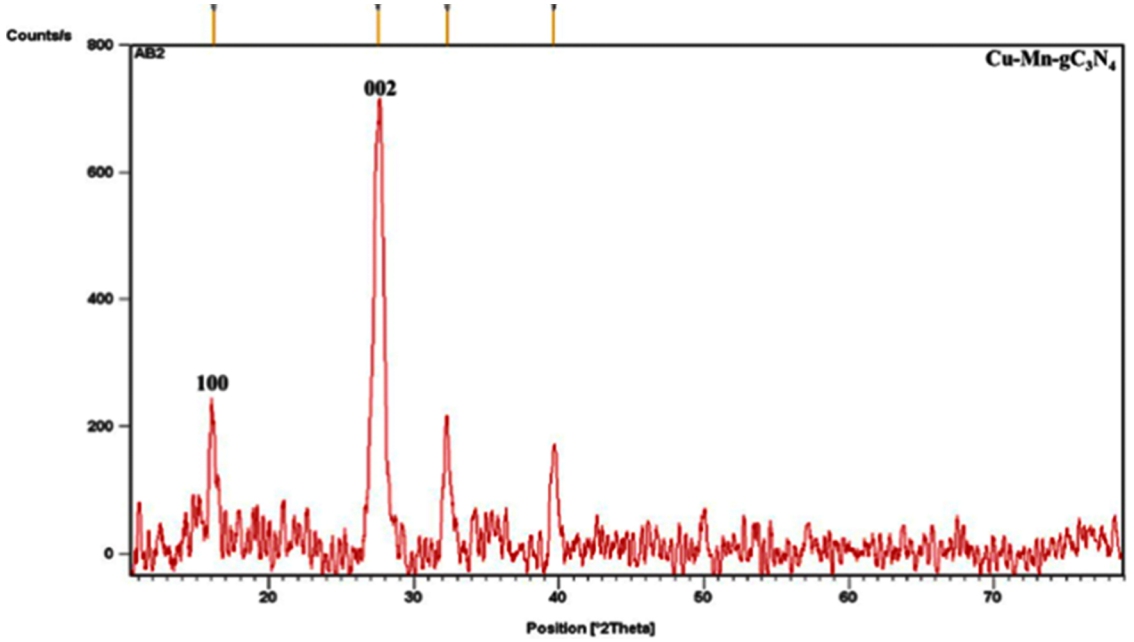

Figure 1. XRD pattern of Cu−Mn−GCN.

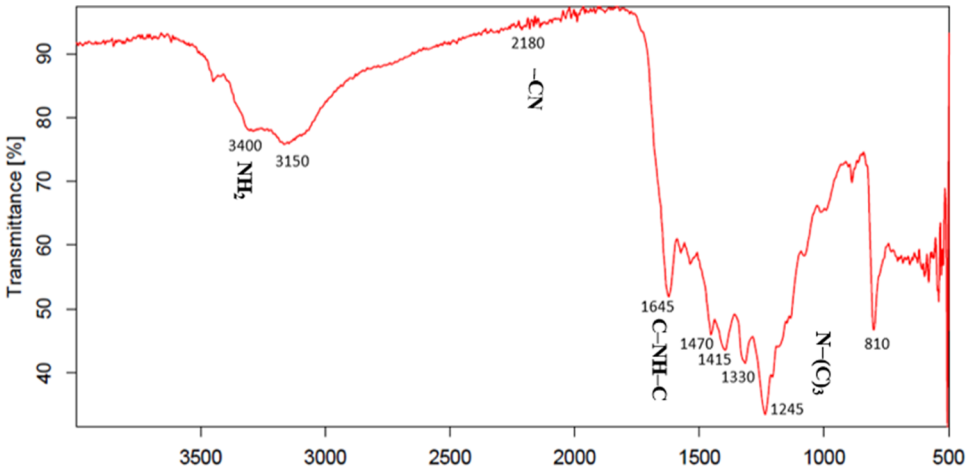

Figure 2. FTIR spectra of Cu−Mn−GCN.

spectroscopy (FTIR), and scanning electron microscopy (SEM) were used to confirm the composition of Cu−Mn-doped GCN.

2. EXPERIMENTAL SECTION

2.1. Raw Materials. Melamine ($C_3H_6N_6$, 99%, DAEJUNG Chemical and Metals Co., Ltd., Korea), nitric acid (HNO_3, 70% Sigma Aldrich), ethylene glycol ($C_2H_6O_2$, Sigma Aldrich, 99%), copper chloride ($CuCl_2$, ALFA AESAR, 99%), ethanol (C_2H_5OH, Sigma Aldrich, 95−100%), MB ($C_{16}H_{18}ClN_3S$, QREC, 30%), hydrogen peroxide (H_2O_2, Sigma Aldrich, 30%), manganese chloride ($MnCl_2$, ALFA AESAR), and distilled water were used.

2.2. Synthesis of Graphitic Carbon Nitride (GCN). The GCN was thermally prepared by melamine self-condensation. 7 g of melamine was taken into a covered ceramic and placed in a muffle furnace at 500 °C for 4 h with a heating rate of 10 °C per minute; after cooling at 25 °C, a canary-yellow solid product was attained.[11] Then, it was ground to the powder form with an agate mortar. In a round-bottom flask (RBF), the powdered product was taken and 5 M nitric acid solution was added; the RBF was placed in an oil bath and refluxed for 24 h at 110 °C. The refluxed solution was then washed with water through centrifugation to bring the pH of the sample to 7. Then, the sample was dried till it was dry.[12]

2.3. Synthesis of Cu−Mn−GCN. Cu−Mn−GCN is synthesized with a very simple method. Three different solutions were prepared, and all these solutions containing 0.5 g (carbon nitride, $CuCl_2$, and $MnCl_2$) were added in 10 mL of distilled water and 10 mL of ethyl glycol. Then, these solutions were sonicated for about 5−10 min. This solution was autoclaved at 160 °C for 16 h. Then, the solution was cooled at room temperature (25 °C), rinsed with distilled water, and dried at vacuum conditions to attain the Cu−Mn−GCN composite.[13]

2.4. Characterization. The crystal structure and phase purity of the synthesized product Cu−Mn−GCN were characterized by XRD.[14] The X-ray diffraction data of Cu−Mn−gC3N4 were collected using a Siemens Diffractometer D5000 diffractometer Kristalloflex, equipped with Cu Kα

https://doi.org/10.1021/acsomega.3c00814
ACS Omega 2023, 8, 19486−19493

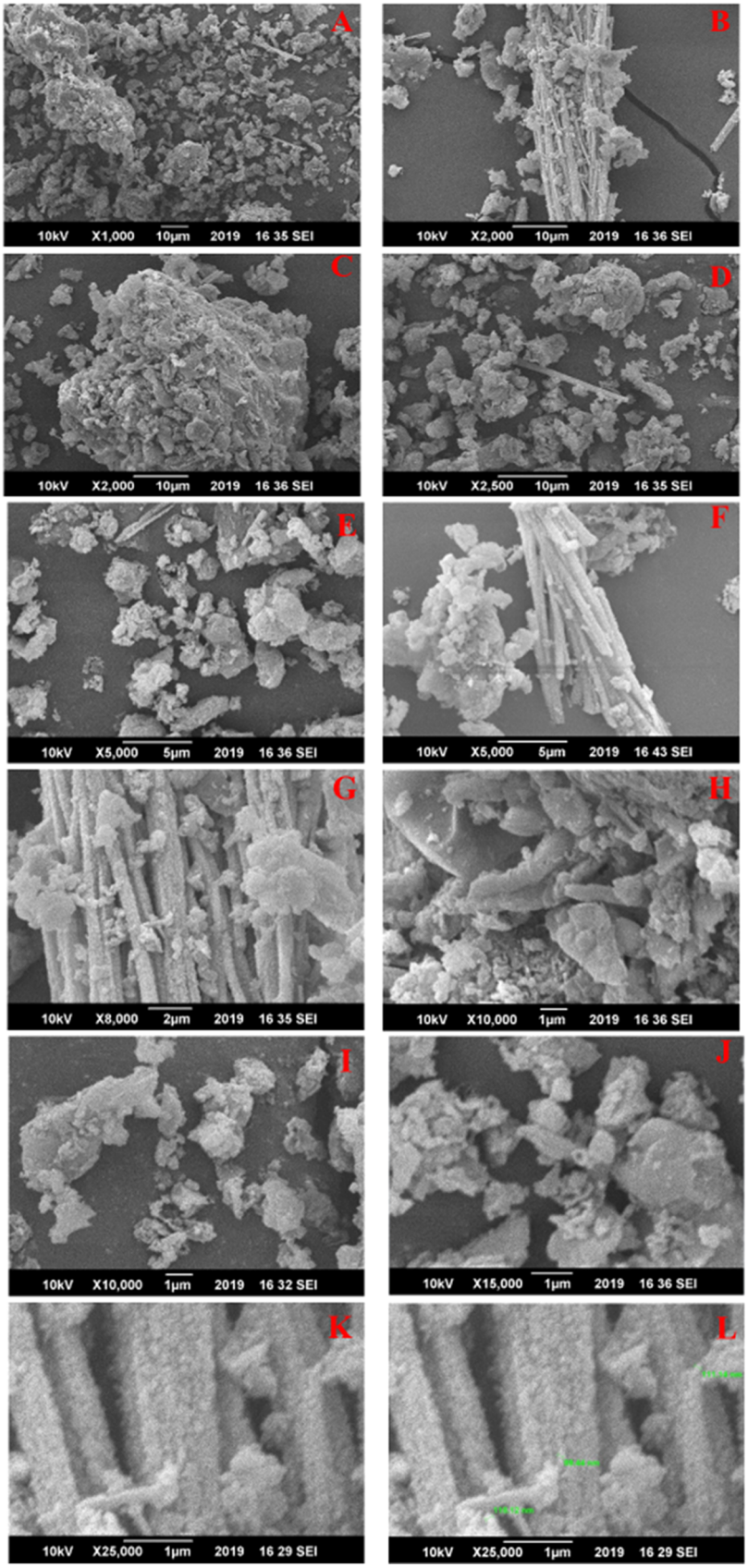

Figure 3. continued

https://doi.org/10.1021/acsomega.3c00814
ACS Omega 2023, 8, 19486−19493

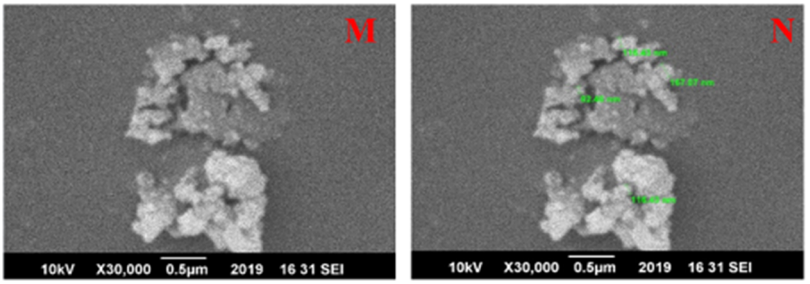

Figure 3. SEM diagrams of Cu−Mn−gC_3N_4 in different magnifications.

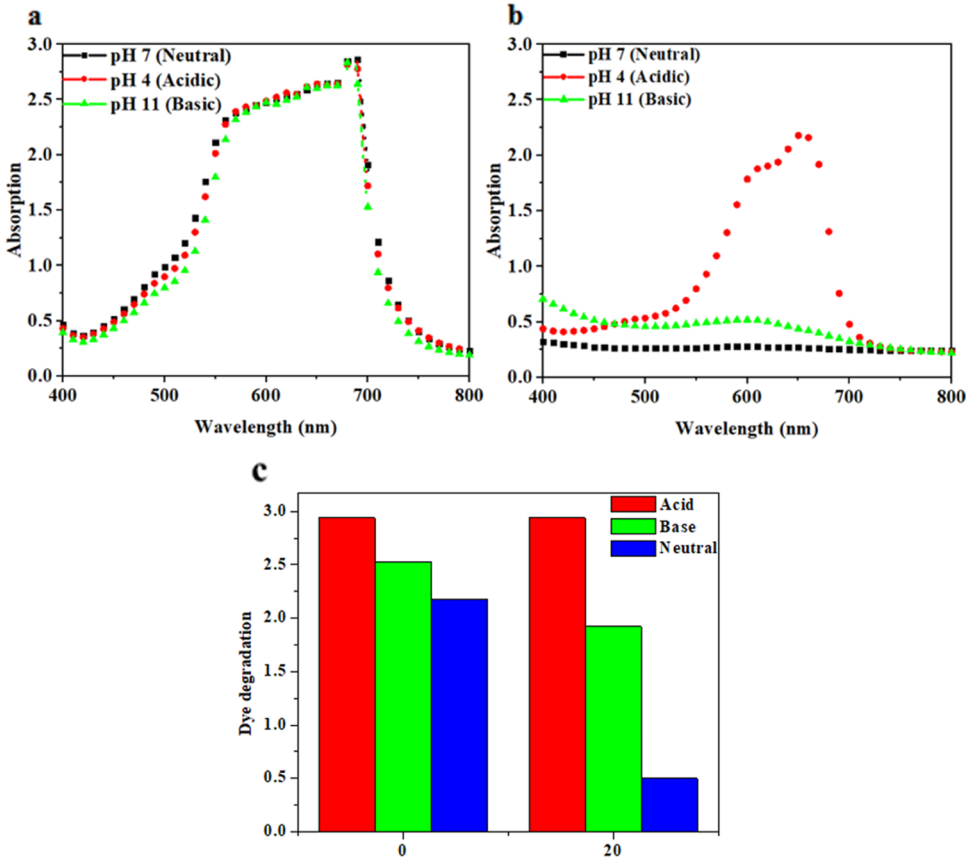

Figure 4. (a) Absorption spectra of different pH values at 0 min. (b) Absorption spectra of different pH values at 20 min. (c) Degradation at different pH values.

radiation, λ = 0.154 nm, FTIR spectra were recorded using a NEXUS 670 spectrometer,[15] UV−visible absorption spectra was characterized using a UV-2450 Shimadzu Vis-spectrometer, a SEM Leica Cambridge was used to study the morphology and surface of the synthesized composite, and UV−visible absorption spectra were collected using a UV-2450 Shimadzu Vis-spectrometer.[14,16]

2.4.1. XRD. The X-ray diffraction (XRD) patterns of Cu−Mn−GCN-500 are displayed in Figure 1. The XRD pattern shows that a diffraction peak at 16.16° was assigned to the crystal plane (100), which was due to the interplanar separation of the tri-s-triazine. The diffraction peak at 27.52°, crystal plane (002), is due to the stacking of the aromatic system present between the carbon nitride (CN) layers. The XRD patterns of the composite displayed that the assigned peaks (100) and (002) exhibited are on the right side, owing to the crystal lattice distortion after Cu−Mn chelation.[17] Two peaks at 32.27 and 39.67° in the XRD pattern confirm the presence of Cu in the composite. In the XRD pattern, Mn species do not display their peak like in manganese chloride, manganese oxide, and manganese nitride and the Cu−Mn−GCN-500 composite. The GCN nanosheet did not hinder the growth of GCN, but when Mn has added, the nature of the material changed from crystalline to amorphous, and it was clear that Mn was present in the coordination form like the Mn−N bond. The presence of Mn and Cu in the composite was also confirmed by scanning electron microscopy (SEM).

2.4.2. FTIR. The FTIR spectrum was used to identify the Cu−Mn−GCN. Two broad peaks are shown in Figure 2 at 3150 and 3400 cm^{-1}, which were caused by the occurrence of secondary and primary amines in the stretching vibration form, respectively. If the absorption peaks were strong, it means that there were many terminal amines. Figure 4 shows that the absorption peaks at 3400 and 3150 cm^{-1} were weak, which means the low quantity of terminal amines. The band between 1200 and 1700 cm^{-1} which includes peaks at 1645, 1470,

https://doi.org/10.1021/acsomega.3c00814
ACS Omega 2023, 8, 19486−19493

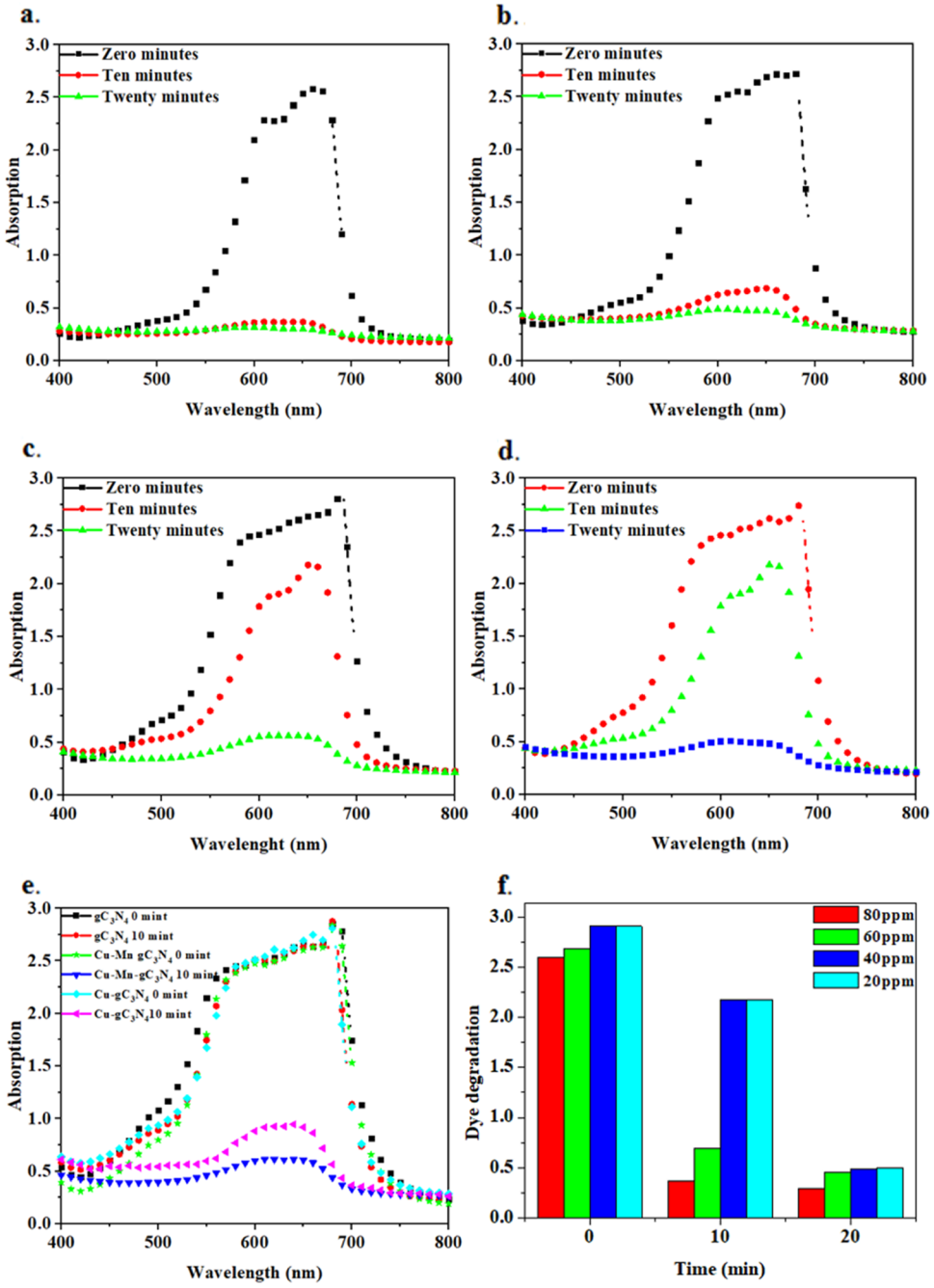

Figure 5. (a) Absorption spectra of different times for 80 ppm solution. (b) Absorption spectra of different times for 60 ppm solution. (c) Absorption spectra of different times for 40 ppm solution. (d) Absorption spectra of different times at 20 ppm. (e) Absorption spectra of different times for combinations. (f) Absorption spectra of different times for combinations.

1415, 1330, and 1245 cm^{-1} was attributed to the stretching vibrations of the connected units of $N-(C)_3$ and C−NH−C for skeletal vibrations of heptazine heterocyclic rings. However, the absorption intensity of Cu−Mn−GCN in this region (1200−1700 cm^{-1}) was less compared to that of pure GCN due to the formation of Cu−Mn−N_x because the bonding between Cu, Mn, and N atoms could lower the stretching vibration of heptazine or triazine rings. The peak at 810 cm^{-1} was attributed to the bending vibration of heptazine and s-triazine ring systems. The peak appearing at 2180 cm^{-1} was due to the Mn-induced surface defect in the −CN group. These peaks revealed embedding of Cu−Mn atoms in the polymerization of melamine, while Cu−Mn−N_x species were formed by coordination of Cu and Mn atoms with the N atoms from the triazine rings[18]

2.4.3. Scanning Electron Microscopy (SEM) and EDX Data. SEM was utilized for exploring the structure as well as the morphology of the Cu−Mn−GCN composite. The presence of GCN nanosheets and Cu−Mn dispersed on GCN at different comparable sizes of 0.5−10 μm and a magnification of X1000−X3000 is characterized by SEM (Figure 3). It was reflected that the structure of GCN was a wrinkled sheet. Cu−Mn doping on GCN nanosheets improves the surface area of the Cu−GCN.[19] EDX data were obtained for the composite, and incorporation of metals in the

https://doi.org/10.1021/acsomega.3c00814
ACS Omega 2023, 8, 19486−19493

nanocomposite was confirmed. The EDX analysis images are shown in Supporting Information S1.

2.4.4. Surface Measurement (Brunauer–Emmett–Teller (BET)). Specific surface area was determined for the composite, which was found to be 88.9 m^2/g, which is a relatively high value for the graphitic carbon nitride composite. It is clear from the previously reported data that bulk g-C_3N_4 possesses small specific surface area, while the improved specific area in the nanocomposite can be attributed to the improved photocatalytic properties. The BET analysis graph is shown in Supporting Information S2.

2.5. Catalytic Performance. *2.5.1. Effect of PH.* The catalytic activity of Cu–Mn–GCN composites was characterized on the conventional organic dye pollutant MB. 100 ppm MB aqueous solution was prepared, and 0.01 g of Cu–Mn–GCN, at neutral PH, was added to 50 milliliters (mL) of 100 parts per million (ppm) MB solution; the second solution was made in acidic conditions at pH 4, and the third was kept at basic conditions at pH 11. A few drops of dilute H_2O_2 were added to each solution. The mixture of Cu–Mn–GCN and MB solution was stirred for 20 min to achieve the equilibrium of adsorption/desorption.

The solutions were retained in a shaker in the presence of sunlight. It was seen that after 20 min, the neutral solution became colorless, and after a long time, the basic solution also became colorless, but no change was noted for the acidic solution. Absorption analysis was performed for all three solutions, and it was noted that the neutral conditions displayed maximum degradation compared to the other two solutions, as shown in Figure 4a–c, at 0 and 20 min.

2.5.2. Effect of Concentration. After 20 min, 10, 30, 70, and 90% MB was degraded for 80, 60, 40, and 20 ppm solution, respectively, (Figure 5a–d). Cu–Mn–GCN and MB solution of the neutral conditions could degrade 100% of the MB within 25 min, and at the basic conditions, 70% of the MB was degraded, but no change for the acidic conditions was observed. 0.01 g of each pure GCN, Cu–GCN, and Cu–Mn–GCN was added to 50 mL of 100 ppm MB solution of neutral conditions. All three solutions were stirred for 20 min to arrive at the equilibrium of adsorption–desorption. A few drops of diluted H_2O_2 were added to each solution. All the solutions were kept in a shaker in the presence of sunlight.

Absorption analysis was performed at 0 min, and at 10 min, it was noted that Cu–Mn–GCN eliminated 90%, Cu–GCN eliminated 75%, and pure GCN did not eliminate MB from the solution. Figure 5e,f illustrates the degradation performance for all pure GCN, Cu–GCN, and Cu–Mn–GCN at 0 and 10 min. 0.01 g of each pure GCN Cu–GCN and Cu–Mn–GCN was added to 50 mL of 100 ppm MB solution of neutral conditions. All three solutions were stirred for 20 min to arrive at the equilibrium of adsorption–desorption. A few drops of dilute H_2O_2 were added to each solution. All the solutions were kept in a shaker in the presence of sunlight. Absorption analysis was performed at 0 min, and at 10 min, it was noted that Cu–Mn–GCN eliminated 90%, Cu–GCN eliminated 75%, and pure GCN did not eliminate MB from the solution.

2.5.2.1. Total Organic Carbon Analysis (TOC). A total organic carbon analyzer (TOC, Shimadzu, TOC-L series) was used to look at the mineralization of Cu–Mn over GCN samples, and more than 50% degradation of total organic carbon was observed. Using a fluorescence spectrophotometer (Hitachi, F-7000), the three-dimensional excitation–emission matrix fluorescence spectra (3D EEMs) were studied. The slit was 10 nm wide, and the excitation (Eex) and emission (Eem) wavelength scanning ranges were 250–400 and 250–500 nm, respectively. Analysis was done to check how well the bare Cu–Mn over GCN catalysts could mineralize. The excitation (Eex) and emission (Eem) wavelength scanning ranges were 250–400 and 250–500 nm, respectively, and the slit was 10 nm wide. Analysis was done to check the bare Cu–Mn over GCN catalysts' potential for mineralization.

3. CONCLUSIONS

In this study, a Mn–Cu-doped GCN composite was developed to be used as a photocatalyst for the degradation of the organic dye MB. The Cn–Mn–GCN-500C composite was synthesized thermally by self-condensation of melamine. The material showed excellent performance for degradation at neutral pH. 0.01 g of Mn–Cu–GCN showed the highest catalytic activity. The experiment was performed with different concentrations of MB solutions of 20, 40, 60, and 80 ppm. The catalyst displayed a higher activity after 15 min in a solution of 20 ppm concentration, and the activity increases with the amount of the catalyst. Hydrogen peroxide (H_2O_2) was used as an initiator for the reaction by providing hydroxyl ions. FTIR spectra of the composite were also recorded as a peak appeared at 2180 cm^{-1} due to the Mn-induced surface defect in the –CN group. These peaks revealed embedding of Cu–Mn atoms in the melamine, while Cu–Mn–N_x species were formed by coordinating Cu and Mn atoms with the N atoms from the triazine rings. Cu–Mn doping on GCN nanosheets improves the surface area of the Cu–GCN. The presence of Mn and Cu in the composite was also confirmed by SEM analysis, which reveals that Mn–Cu doping with GCN increases its surface area. XRD analysis confirms the presence of the Mn–N bond and the change of the structure from crystalline to amorphous after doping. These calculations show that the prepared Mn–Cu possesses good catalytic activity and is a good candidate for the environmental remediation sector.

■ ASSOCIATED CONTENT

Supporting Information

The Supporting Information is available free of charge at https://pubs.acs.org/doi/10.1021/acsomega.3c00814.

(PDF)

■ AUTHOR INFORMATION

Corresponding Authors

Hui Li – *Key Laboratory of Clusters Science of Ministry of Education, School of Chemistry and Chemical Engineering, Beijing Institute of Technology, Beijing 100081, P. R. China;* orcid.org/0000-0001-7459-6618; Email: lihui@bit.edu.cn

Javed Iqbal – *Department of Chemistry, University of Agriculture, 38000 Faisalabad, Pakistan; Department of Chemistry, College of Science, University of Bahrain, Sakhir 32038, Bahrain;* orcid.org/0000-0003-0598-8401; Email: Javedkhattak79@gmail.com, Javed.iqbal@uaf.edu.pk, Jiqbal@uob.edu.bh

Authors

Ali Raza Ayub – *Key Laboratory of Clusters Science of Ministry of Education, School of Chemistry and Chemical Engineering, Beijing Institute of Technology, Beijing 100081, P. R. China*

https://doi.org/10.1021/acsomega.3c00814
ACS Omega 2023, 8, 19486–19493

Asmat Ullah − *Department of Chemistry, University of Agriculture, 38000 Faisalabad, Pakistan*
Faisal Nawaz − *Department of Basic Sciences & Humanities, UET (Lahore) Faisalabad Campus, 38000 Faisalabad, Pakistan*
Saqib Shafiq − *Department of Chemistry, University of Agriculture, 38000 Faisalabad, Pakistan*
Ahmed Abd El-Fattah − *Department of Chemistry, College of Science, University of Bahrain, Sakhir 32038, Bahrain; Department of Materials Science, Institute of Graduate Studies and Research, Alexandria University, Alexandria 21526, Egypt*

Complete contact information is available at: https://pubs.acs.org/10.1021/acsomega.3c00814

Notes

The authors declare no competing financial interest.

■ ACKNOWLEDGMENTS

The authors acknowledge the financial and technical support from the Punjab Bio-energy Institute (PBI) and the University of Agriculture Faisalabad (UAF).

■ REFERENCES

(1) (a) Molinari, R.; Grande, C.; Drioli, E.; Palmisano, L.; Schiavello, M. Photocatalytic membrane reactors for degradation of organic pollutants in water. *Catal. Today* **2001**, *67*, 273−279. (b) Molinari, R.; Borgese, M.; Drioli, E.; Palmisano, L.; Schiavello, M. Hybrid processes coupling photocatalysis and membranes for degradation of organic pollutants in water. *Catal. Today* **2002**, *75*, 77−85.

(2) (a) Li, S.; Zhao, Z.; Yu, D.; Zhao, J.-Z.; Su, Y.; Liu, Y.; Lin, Y.; Liu, W.; Xu, H.; Zhang, Z. Few-layer transition metal dichalcogenides (MoS2, WS2, and WSe2) for water splitting and degradation of organic pollutants: Understanding the piezocatalytic effect. *Nano Energy* **2019**, *66*, No. 104083. (b) Sheng, H.; Li, Q.; Ma, W.; Ji, H.; Chen, C.; Zhao, J. Photocatalytic degradation of organic pollutants on surface anionized TiO2: Common effect of anions for high hole-availability by water. *Appl. Catal., B* **2013**, *138−139*, 212−218. (c) Černigoj, U.; Štangar, U. L.; Trebše, P. Evaluation of a novel Carberry type photoreactor for the degradation of organic pollutants in water. *J. Photochem. Photobiol., A* **2007**, *188*, 169−176.

(3) (a) Cao, S.; Low, J.; Yu, J.; Jaroniec, M. Polymeric photocatalysts based on graphitic carbon nitride. *Adv. Mater.* **2015**, *27*, 2150−2176. (b) Wang, X.; Blechert, S.; Antonietti, M. Polymeric graphitic carbon nitride for heterogeneous photocatalysis. *ACS Catal.* **2012**, *2*, 1596−1606.

(4) Akhundi, A.; Badiei, A.; Ziarani, G. M.; Habibi-Yangjeh, A.; Munoz-Batista, M. J.; Luque, R. Graphitic carbon nitride-based photocatalysts: toward efficient organic transformation for value-added chemicals production. *Mol. Catal.* **2020**, *488*, No. 110902.

(5) (a) Wang, W.; Yu, J. C.; Xia, D.; Wong, P. K.; Li, Y. Graphene and g-C3N4 nanosheets cowrapped elemental α-sulfur as a novel metal-free heterojunction photocatalyst for bacterial inactivation under visible-light. *Environ. Sci. Technol.* **2013**, *47*, 8724−8732. (b) Wang, W.; Li, G.; An, T.; Chan, D. K.; Jimmy, C. Y.; Wong, P. K. Photocatalytic hydrogen evolution and bacterial inactivation utilizing sonochemical-synthesized g-C3N4/red phosphorus hybrid nanosheets as a wide-spectral-responsive photocatalyst: the role of type I band alignment. *Appl. Catal., B* **2018**, *238*, 126−135. (c) Li, G.; Nie, X.; Chen, J.; Jiang, Q.; An, T.; Wong, P. K.; Zhang, H.; Zhao, H.; Yamashita, H. Enhanced visible-light-driven photocatalytic inactivation of *Escherichia coli* using g-C3N4/TiO2 hybrid photocatalyst synthesized using a hydrothermal-calcination approach. *Water Res.* **2015**, *86*, 17−24. (d) Zhang, C.; Li, Y.; Shuai, D.; Shen, Y.; Xiong, W.; Wang, L. Graphitic carbon nitride (g-C3N4)-based photocatalysts for water disinfection and microbial control: A review. *Chemosphere* **2019**, *214*, 462−479. (e) Kang, S.; Huang, W.; Zhang, L.; He, M.; Xu, S.; Sun, D.; Jiang, X. Moderate bacterial etching allows scalable and clean delamination of g-C3N4 with enriched unpaired electrons for highly improved photocatalytic water disinfection. *ACS Appl. Mater. Interfaces* **2018**, *10*, 13796−13804.

(6) Sabri, M.; Habibi-Yangjeh, A.; Rahim Pouran, S.; Wang, C. Titania-activated persulfate for environmental remediation: the-state-of-the-art. *Catal. Rev.* **2021**, *65*, 1−56.

(7) (a) Wu, M.; Yan, J.-M.; Zhang, X.-w.; Zhao, M. Synthesis of g-C3N4 with heating acetic acid treated melamine and its photocatalytic activity for hydrogen evolution. *Appl. Surf. Sci.* **2015**, *354*, 196−200. (b) Vu, N. N.; Nguyen, C. C.; Kaliaguine, S.; Do, T. O. Synthesis of g-C3N4 nanosheets by using a highly condensed lamellar crystalline melamine−cyanuric acid supramolecular complex for enhanced solar hydrogen generation. *ChemSusChem* **2019**, *12*, 291−302. (c) Kiasat, A. R.; Fallah-Mehrjardi, M. Melamine sulfonic acid: a recoverable catalyst for the ecofriendly synthesis of thiocyanohydrins under solvent-free conditions. *Synth. Commun.* **2010**, *40*, 1551−1558.

(8) Lu, D.; Wang, H.; Zhao, X.; Kondamareddy, K. K.; Ding, J.; Li, C.; Fang, P. Highly efficient visible-light-induced photoactivity of Z-scheme g-C3N4/Ag/MoS2 ternary photocatalysts for organic pollutant degradation and production of hydrogen. *ACS Sustainable Chem. Eng.* **2017**, *5*, 1436−1445.

(9) Dar, A. A.; Usman, M.; Zhang, W.; Zhu, Q.; Pan, B.; Sial, A.; Wang, C. Synergistic degradation of 2, 4, 4′-trihydroxybenzophenone using carbon quantum dots, ferrate, and visible light irradiation: Insights into electron generation/consumption mechanism. *ACS ES&T Engg.* **2022**, *2*, 1942−1952.

(10) (a) Li, H.; Shan, C.; Pan, B. Fe (III)-doped g-C3N4 mediated peroxymonosulfate activation for selective degradation of phenolic compounds via high-valent iron-oxo species. *Environ. Sci. Technol.* **2018**, *52*, 2197−2205. (b) An, S.; Zhang, G.; Wang, T.; Zhang, W.; Li, K.; Song, C.; Miller, J. T.; Miao, S.; Wang, J.; Guo, X. High-density ultra-small clusters and single-atom Fe sites embedded in graphitic carbon nitride (g-C3N4) for highly efficient catalytic advanced oxidation processes. *ACS Nano* **2018**, *12*, 9441−9450. (c) Nie, Y.-C.; Yu, F.; Wang, L.-C.; Xing, Q.-J.; Liu, X.; Pei, Y.; Zou, J.-P.; Dai, W.-L.; Li, Y.; Suib, S. L. Photocatalytic degradation of organic pollutants coupled with simultaneous photocatalytic H2 evolution over graphene quantum dots/Mn-N-TiO2/g-C3N4 composite catalysts: Performance and mechanism. *Appl. Catal., B* **2018**, *227*, 312−321. (d) Chen, Y.; Lu, W.; Shen, H.; Gu, Y.; Xu, T.; Zhu, Z.; Wang, G.; Chen, W. Solar-driven efficient degradation of emerging contaminants by g-C3N4-shielding polyester fiber/TiO2 composites. *Appl.Catal., B* **2019**, *258*, No. 117960. (e) Wang, Y.; Zhao, X.; Cao, D.; Wang, Y.; Zhu, Y. Peroxymonosulfate enhanced visible light photocatalytic degradation bisphenol A by single-atom dispersed Ag mesoporous g-C3N4 hybrid. *Appl. Catal., B* **2017**, *211*, 79−88. (f) Lu, D.; Zhang, G.; Wan, Z. Visible-light-driven g-C3N4/Ti3+-TiO2 photocatalyst co-exposed {0 0 1} and {1 0 1} facets and its enhanced photocatalytic activities for organic pollutant degradation and Cr (VI) reduction. *Appl. Surf. Sci.* **2015**, *358*, 223−230.

(11) (a) Dyjak, S.; Kiciński, W.; Huczko, A. Thermite-driven melamine condensation to C x N y H z graphitic ternary polymers: towards an instant, large-scale synthesis of gC 3 N 4. *J. Mater. Chem. A* **2015**, *3*, 9621−9631. (b) Iqbal, W.; Dong, C.; Xing, M.; Tan, X.; Zhang, J. Eco-friendly one-pot synthesis of well-adorned mesoporous gC 3 N 4 with efficiently enhanced visible light photocatalytic activity. *Catal. Sci. Technol.* **2017**, *7*, 1726−1734.

(12) (a) Ong, W.-J.; Tan, L.-L.; Ng, Y. H.; Yong, S.-T.; Chai, S.-P. Graphitic carbon nitride (g-C3N4)-based photocatalysts for artificial photosynthesis and environmental remediation: are we a step closer to achieving sustainability? *Chem. Rev.* **2016**, *116*, 7159−7329. (b) Wang, Y.; Tan, G.; Liu, T.; Su, Y.; Ren, H.; Zhang, X.; Xia, A.; Lv, L.; Liu, Y. Photocatalytic properties of the g-C3N4/{010} facets BiVO4 interface Z-Scheme photocatalysts induced by BiVO4 surface heterojunction. *Appl. Catal., B* **2018**, *234*, 37−49.

(13) (a) Cui, Y.; Zhang, J.; Zhang, G.; Huang, J.; Liu, P.; Antonietti, M.; Wang, X. Synthesis of bulk and nanoporous carbon nitride polymers from ammonium thiocyanate for photocatalytic hydrogen evolution. *J. Mater. Chem.* **2011**, *21*, 13032−13039. (b) Cheng, C.; Huang, Y.; Tian, X.; Zheng, B.; Li, Y.; Yuan, H.; Xiao, D.; Xie, S.; Choi, M. M. Electrogenerated chemiluminescence behavior of graphite-like carbon nitride and its application in selective sensing Cu2+. *Anal. Chem.* **2012**, *84*, 4754−4759.

(14) (a) Fina, F.; Callear, S. K.; Carins, G. M.; Irvine, J. T. Structural investigation of graphitic carbon nitride via XRD and neutron diffraction. *Chem. Mater.* **2015**, *27*, 2612−2618. (b) Guo, Q.; Xie, Y.; Wang, X.; Lv, S.; Hou, T.; Liu, X. Characterization of well-crystallized graphitic carbon nitride nanocrystallites via a benzene-thermal route at low temperatures. *Chem. Phys. Lett.* **2003**, *380*, 84−87.

(15) Ben-Refael, A.; Benisti, I.; Paz, Y. Transient photoinduced phenomena in graphitic carbon nitride as measured at nanoseconds resolution by step-scan FTIR. *Catal. Today* **2020**, *340*, 97−105.

(16) Li, C.; Cao, C.-B.; Zhu, H.-S. Graphitic carbon nitride thin films deposited by electrodeposition. *Mater. Lett.* **2004**, *58*, 1903−1906.

(17) (a) Mousavi, M.; Habibi-Yangjeh, A. Integration of NiWO 4 and Fe 3 O 4 with graphitic carbon nitride to fabricate novel magnetically recoverable visible-light-driven photocatalysts. *J. Mater. Sci.* **2018**, *53*, 9046−9063. (b) Yu, Z.; Li, F.; Yang, Q.; Shi, H.; Chen, Q.; Xu, M. Nature-mimic method to fabricate polydopamine/graphitic carbon nitride for enhancing photocatalytic degradation performance. *ACS Sustainable Chem. Eng.* **2017**, *5*, 7840−7850. (c) Lu, Q.; Deng, J.; Hou, Y.; Wang, H.; Li, H.; Zhang, Y. One-step electrochemical synthesis of ultrathin graphitic carbon nitride nanosheets and their application to the detection of uric acid. *Chem. Commun.* **2015**, *51*, 12251−12253. (d) Jourshabani, M.; Shariatinia, Z.; Badiei, A. Facile one-pot synthesis of cerium oxide/sulfur-doped graphitic carbon nitride (g-C3N4) as efficient nano-photocatalysts under visible light irradiation. *J. Colloid Interface Sci.* **2017**, *507*, 59−73.

(18) (a) Akhundi, A.; Habibi-Yangjeh, A. Graphitic carbon nitride nanosheets decorated with CuCr2O4 nanoparticles: novel photocatalysts with high performances in visible light degradation of water pollutants. *J. Colloid Interface Sci.* **2017**, *504*, 697−710. (b) Ong, W.-J.; Tan, L.-L.; Chai, S.-P.; Yong, S.-T.; Mohamed, A. R. Surface charge modification via protonation of graphitic carbon nitride (g-C3N4) for electrostatic self-assembly construction of 2D/2D reduced graphene oxide (rGO)/g-C3N4 nanostructures toward enhanced photocatalytic reduction of carbon dioxide to methane. *Nano Energy* **2015**, *13*, 757−770.

(19) Cui, Y.; Tang, Y.; Wang, X. Template-free synthesis of graphitic carbon nitride hollow spheres for photocatalytic degradation of organic pollutants. *Mater. Lett.* **2015**, *161*, 197−200.

https://doi.org/10.1021/acsomega.3c00814
ACS Omega 2023, 8, 19486−19493